

## 25% Efficiency Amorphous/Crystalline Heterostructure Solar Cells Based On N-Type Crystalline Silicon

A. Bensaad<sup>1</sup>, Z. Bensaad<sup>2</sup>, B. Soudini<sup>3</sup>, A. Beloufa<sup>4</sup>

*\*Applied Materials Laboratory, Centre de Recherches (ex-CFTE),  
University of Sidi Bel Abbès, 22000 Sidi Bel Abbès, Algeria*

**ABSTRACT:-** In this work we describe in detail the process used to obtain high efficiency amorphous/crystalline silicon heterostructure solar cells, based on n-type crystalline silicon substrate. Numerical simulations with the Analysis of Microelectronic and Photonic Structure (AMPS) program have been carried out to study the stacked TCO/ p-type a-Si:H/ buffer/n-type c-Si/buffer/n-type a-Si:H/Al heterojunction (HJ) silicon solar cells. The influence of various parameters such as thicknesses and doping concentrations of all layers were investigated leading to optimal values of the simulated devices. The results obtained are our best solar cell structures with 25.021% of efficiency and Fill Factor (FF) of 84.4%, respectively. The current density  $J_{sc}$  attains the value of 32.948mA/cm<sup>2</sup> and the open-circuit voltage  $V_{oc}$  the value of 0.899V.

**Keywords:-** Heterojunction solar cells; a-Si:H/c-Si; AMPS-1D ; Amorphous silicon; Defects; Passivation.

### I. INTRODUCTION

The amorphous/crystalline silicon (a-Si/c-Si) hetero-junction (HJ) solar cell is one of the most interesting technological solutions for the photovoltaic market due to their high stability, high conversion efficiencies and low temperature processing which leads to a fabrication cost reduction in comparison with the high temperature diffused homo-junction technology [1,2]. The original design was developed by SANYO Ltd. using n-type substrate as the absorber for the Hetero-junction with intrinsic thin-layer (HIT) solar cell [3]. High efficiency a-Si:H/c-Si HJ solar cells based on n-type Czochralski Si wafers have been successfully introduced by Sawada et al. in 1994 [4]. However, high bulk and surface recombination rates are known to limit the open-circuit voltage and to reduce the fill factor of photovoltaic devices.

The carrier transport and photovoltaic properties of these solar cells are significantly affected by band offset and interface defects [5-6-7]. Different techniques for obtaining a high quality interface can be used including bandgap grading and passivation of the interface states by chemical HF etching, atomic hydrogen treatment, and deposition of an a-Si:H passivation layer [8-9-10]. Surface passivation of the c-Si wafer is one of most important steps to obtain higher minority carrier lifetime and open circuit voltage. A very high open-circuit voltages  $V_{oc}$  can be achieved by excellent surface passivation properties of the thin hydrogenated amorphous silicon (a-Si:H) films which can be grown by plasma-enhanced chemical vapor deposition (PECV) at low temperatures (200°C).

For single crystalline silicon solar cells, high energy conversion efficiency has been demonstrated using passivation. A higher conversion efficiency of 24.7% was obtained with a thin wafer of 98  $\mu\text{m}$  [11]. The surface defects at the c-Si/a-Si:H interface decreases by inserting an intrinsic a-Si:H(i) buffer layer leading to a significant optimization of the device. The commonly passivation schemes in photovoltaic applications use silicon dioxide (SiO<sub>2</sub>) [12-13], silicon nitride (SiN<sub>x</sub>) [14-15], and amorphous silicon carbide (a-SiC:H) [21-22].

In this paper, we will present numerical simulations for the stacked TCO/ p-type a-Si:H/ buffer/n-type c-Si/buffer/n-type a-Si:H/Al hetero-junction (HJ) silicon solar cells and discuss their possibilities and limitations. The analysis of microelectronic and photonic structure (AMPS) program has been utilized to analyze the characteristics of photovoltaic devices by simulations [19]. The influence of the emitter layer, intrinsic layer and crystalline Si layer on the solar cell performance is investigated by means of modeling and numerical computer simulations for different parameters. The films with boron content higher than  $3 \times 10^{20}$  atoms/cm<sup>3</sup> were excluded in this work because at about this concentration the optical and structural properties start to change significantly. In particular, the hydrogen concentration and band gap decrease as the boron concentration increases in that range [17].

## II. LAYER STRUCTURES MODEL

AMPS-1D is a very general computer simulation code developed by a group from Pennsylvania State University for analyzing and designing two terminal structures [19]. The one-dimensional device simulation program AMPS-1D solves the Poisson's equation and the electron and hole continuity equations by using finite differences and the Newton-Raphson technique. The structure solar cell models have been designed and analyzed the performance in respect to the Voc, Jsc, FF and efficiency by incorporating the material parameters into AMPS-1D.

In this work, the hetero-structure is a stacked structure of TCO/ a-Si:H(p+)/ buffer/ c-Si(n)/buffer/ a-Si:H(n)/Al layer, is investigated. A schematic diagram of this device is shown in Fig. 1. The transparent conductive oxide (TCO) layer is deposited on top of the structure in order to increase the collection and to perform the antireflection layer. The value of TCO is chosen to obtain the highest quality solar cells. The application of the TCO layer provides a less resistive path to transport photo-generated charge carriers to the metal contacts. The resistivity of ITO is as low as  $2.3 \times 10^{-4} \Omega\text{-cm}$  and optical transmittance in the visible wavelength range above 90%. Moreover, a key advantage of ITO is that it is physically stable and chemically inert [20].

TCO $\phi=5.2\text{eV}$
a_Si :H(p+)
Thickness 5nm
Buffer layer
Thickness 5nm
c_Si(n)
Thickness 50 $\mu\text{m}$
Buffer layer
Thickness 5nm
a_Si :H(n+)
Thickness 10nm
Al

Fig. 1. Schematic diagram of our best cell structures parameters used in AMPS program.

A thin amorphous intrinsic buffer layers (5nm) is inserted at the amorphous/c-Si interface to suppress the carrier recombination at this junction. The back contact is realized by an hetero-junction c-Si(n)/a-Si:H(i)/a-Si:H(n+).

In this way a very low recombination rate at back contact occurs and a better collection is obtained. Each layer of the device has been described by a set of parameters to define semiconductor properties. In particular we take into account the thickness, doping level, absorption coefficient, energy gap, electron affinity, density of states (DoS) inside the gap and other amorphous and c-Si properties which have been assumed on the basis of literature [7-18]. The parameters used in each layer of the simulated solar cells are summarized in Table I.

Material Parameters	a-Si:H(p+)	a-Si:H(i)	a-Si:H(n+)	c-Si(n)
Thickness (nm)	5-20	5-20	5-20	$5 \times 10^4 - 5 \times 10^5$
Dielectric constant	11.9	11.9	11.9	11.9
Electron affinity(eV)	3.9	3.9	3.9	4.05
Band gap(eV)	1.72	1.72	1.72	1.12
Effective conduction band density ( $\text{cm}^{-3}$ )	$2.50 \times 10^{20}$	$2.50 \times 10^{20}$	$2.50 \times 10^{20}$	$2.80 \times 10^{19}$
Effective valence band density ( $\text{cm}^{-3}$ )	$2.50 \times 10^{20}$	$2.50 \times 10^{20}$	$2.50 \times 10^{20}$	$1.04 \times 10^{19}$
Electron mobility ( $\text{cm}^2 \text{V}^{-1} \text{s}^{-1}$ )	10	20	10	1350
Hole mobility( $\text{cm}^2 \text{V}^{-1} \text{s}^{-1}$ )	1	2	1	450
Acceptor concentration ( $\text{cm}^{-3}$ )	$1 \times 10^{18} - 1 \times 10^{22}$	0	0	0
Donor concentration ( $\text{cm}^{-3}$ )	0	0	$1 \times 10^{18} - 5 \times 10^{22}$	$1 \times 10^{15} - 1 \times 10^{19}$
Band tail density of states ( $\text{cm}^{-3} \text{eV}^{-1}$ )	$2 \times 10^{21}$	$2 \times 10^{21}$	$2 \times 10^{21}$	$1 \times 10^{14}$
Characteristic energy(eV)for donors, acceptors	0.06, 0.03	0.06, 0.03	0.06, 0.03	0.01, 0.01
Capture cross-section for donor states, e, h ( $\text{cm}^2$ )	$1 \times 10^{-15}, 1 \times 10^{-17}$			
Capture cross-section for acceptor states, e, h ( $\text{cm}^2$ )	$1 \times 10^{-17}, 1 \times 10^{-15}$			
Gaussian density of states NDB ( $\text{cm}^{-3}$ )	$8 \times 10^{17}, 5 \times 10^{20}$	$8 \times 10^{15}, 8 \times 10^{17}$	$8 \times 10^{17}, 5 \times 10^{20}$	
Gaussian peak energy(eV) donors, acceptors	1.22, 070	1.22, 070	1.22, 070	
Standard deviation (eV)	0.23	0.23	0.23	
Capture cross section for donor states, e, h ( $\text{cm}^2$ )	$1 \times 10^{-14}, 1 \times 10^{-15}$	$1 \times 10^{-14}, 1 \times 10^{-15}$	$1 \times 10^{-14}, 1 \times 10^{-15}$	
Capture cross-section for acceptor states, e, h ( $\text{cm}^2$ )	$1 \times 10^{-15}, 1 \times 10^{-14}$	$1 \times 10^{-15}, 1 \times 10^{-14}$	$1 \times 10^{-15}, 1 \times 10^{-14}$	

The states are modeled using the defect pool model for the carrier recombination in the a-Si:H bulk and at the a-Si:H/c-Si interface (Table II). The dangling bonds are represented by two Gaussian type functions, which correspond to the donor like (+/0, positively charged to neutral transition) and the acceptor like (0/−, neutral to negatively charged transition) of the amphoteric dangling silicon bonds [3-16]. Both of these acceptor and donor like states consist of exponential band tail states (Urbach tails) and Gaussian mid-gap states (silicon dangling bonds).

Material Parameters	c-Si(n)	Interface defect density	a-Si:H/c-Si
Midgap density of states in c-Si ( $\text{cm}^{-3}\text{eV}^{-1}$ )	$1 \times 10^{11}$	Thickness (nm)	3
Switch-over energy (eV)	0.56	Total interface density of states $D_{it}$ ( $\text{cm}^{-2}$ )	$1 \times 10^9 - 1 \times 10^{13}$
Capture cross-section for donor states, e, h ( $\text{cm}^2$ )	$1 \times 10^{-15}$ , $1 \times 10^{-17}$	Capture cross-section for donor states, e, h ( $\text{cm}^2$ )	$1 \times 10^{-15}$ , $1 \times 10^{-17}$
Capture cross-section for acceptor states, e, h	$1 \times 10^{-17}$ , $1 \times 10^{-15}$	Capture cross-section for acceptor states, e, h ( $\text{cm}^2$ )	$1 \times 10^{-17}$ , $1 \times 10^{-15}$

Table II. Defect parameters.

For the crystalline silicon, defect density is chosen as single defect at 0.56 eV with a total density of interface states  $D_{it}$  of  $1.10^{11}\text{cm}^{-2}$ . Surface recombination velocities of the electrons and holes were set as  $1.10^7\text{cm/s}$ . The light reflection on the front and back contact was set to be 0.1 and 1, respectively.

### III. RESULTS AND DISCUSSION

#### III.1. Effect of silicon film thickness

For numerical simulations, parameters of Table I were used in AMPS-1D program for our TCO/ a-Si:H(p)/ buffer/ c-Si(n)/buffer/ a-Si:H(n)/Al hetero-structure solar cells at one sun ( $100\text{ mW/cm}^2$  light intensity) and  $25^\circ\text{C}$ . The simulation cell results as function of c-Si(n) layer thickness which is varied in the range of  $5 \times 10^4\text{ nm}$  to  $5 \times 10^5$  are displayed in Fig. 2.

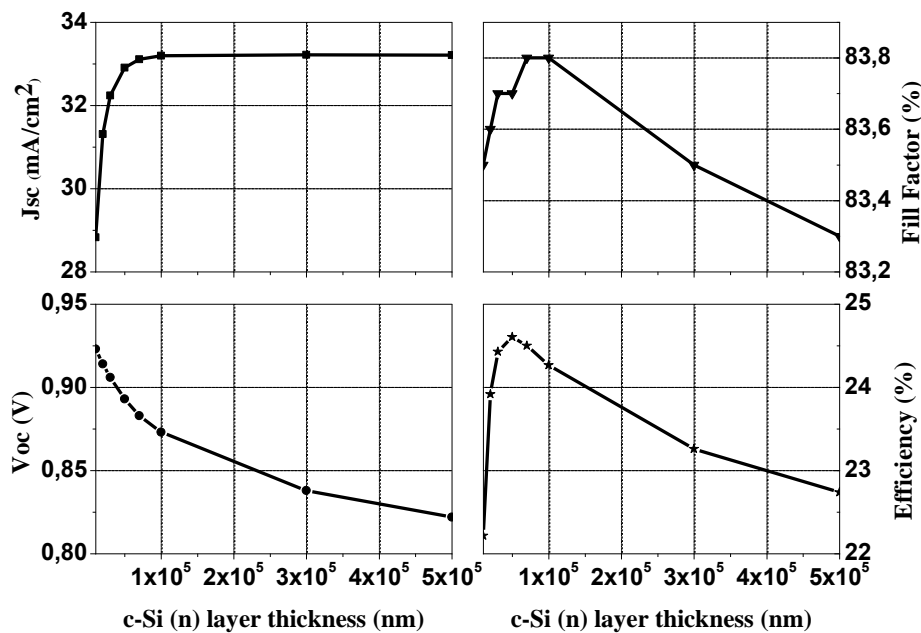


Fig. 2. Current density  $J_{sc}$ , Open-circuit voltage  $V_{oc}$ , Fill Factor FF and conversion Efficiency as function of the c-Si(n) layer thickness.

The results show the dependencies of solar cell performances on the thickness of the c-Si(n) layer for the Heterojunction structure. As it can be seen, the best thickness for the c-Si(n) layer is obtained with the value of  $5 \times 10^4\text{ nm}$  which is thick enough for absorbing light.

### III. 2. Effect of silicon film doping concentration

In order to find the best parameter fitting values for the c-Si(n) doping concentration layer and its effects on the heterostructure solar cells, Fig. 3 and Fig. 4 are drawn by varying the concentration from  $1.10^{15} \text{cm}^{-3}$  to  $1.10^{19} \text{cm}^{-3}$ . The efficiency increases from 24.603% at  $1.10^{15} \text{cm}^{-3}$  to attain the maximum value of 24.641% at  $5.10^{16} \text{cm}^{-3}$  and decreases when the doping concentration is larger than this value. As a result of this observation, the doping concentration of c-Si (n) layer has been chosen as  $5 \cdot 10^{16} \text{cm}^{-3}$

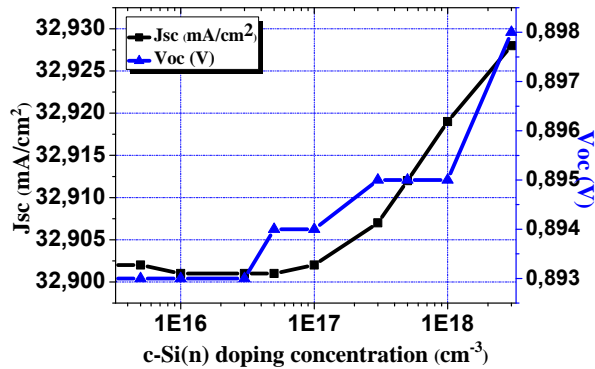


Fig. 3. Current density  $J_{sc}$  and Open-circuit voltage  $V_{oc}$  as function of the c-si(n) layer doping concentration.

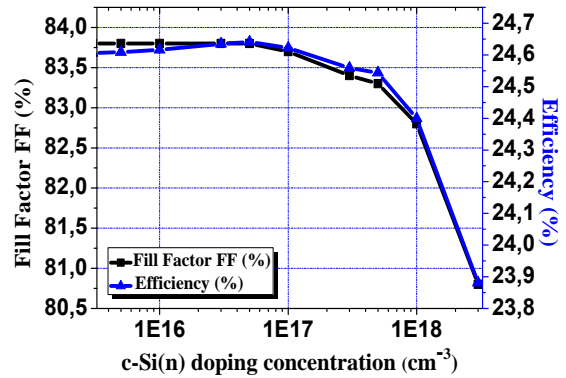


Fig. 4. Fill Factor FF and conversion efficiency as function of the c-si(n) layer doping concentration.

### III. 3. Effect of p-type and n-type layers thickness

The Heterojunction solar cells with different a-Si:H(p+) and a-Si:H(n+) layers thicknesses from 5nm to 40nm and with a 10 nm a-Si:H(i) intrinsic buffer layer at the interface were simulated. As shown in Fig. 5, the current density  $J_{sc}$  is strongly enhanced when the thickness of a-Si:H(p+) layer is decreasing, whereas the maximum open-circuit voltage  $V_{oc}$  value is limited at 10nm. The FF values are independent of the p-layer thickness when the value is larger than 10nm and attain the maximum value at 5nm. The reduction of the emitter thickness results in an increase of the efficiency up to 24.687%. The  $J_{sc}$  decreases from  $32.983 \text{mA/cm}^2$  to  $32.258 \text{mA/cm}^2$  while emitter thickness increases from 5nm to 40 nm.

The  $V_{oc}$  increasing is due to the surface passivation improvement for thicker a-Si:H (i) layers while the  $J_{sc}$  is decreasing with increasing a-Si:H(i) layer thickness. The cause for the short circuit current decreasing is the higher absorption and the absorption losses in the front TCO. The  $J_{sc}$ ,  $V_{oc}$ , FF and conversion efficiency are influenced only little by the a-Si:H(n+) layer thickness.

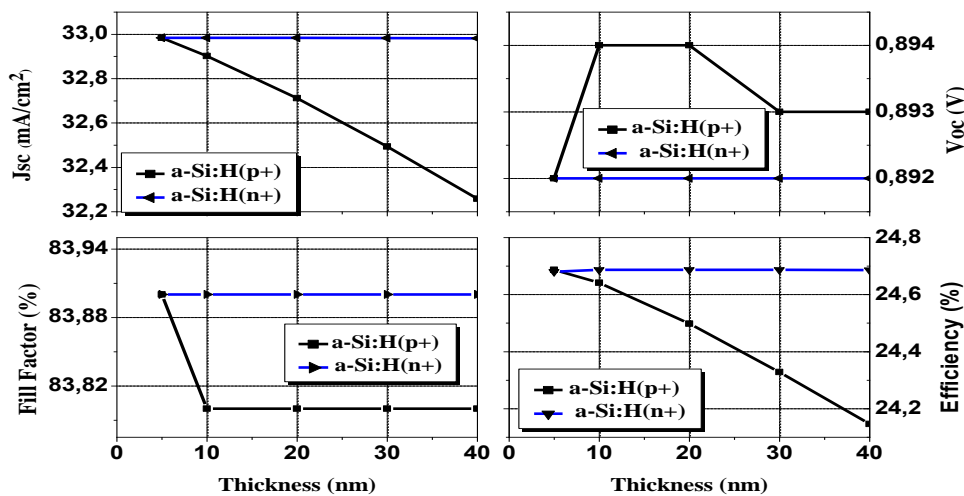


Fig. 5. Current density  $J_{sc}$ , Open-circuit voltage  $V_{oc}$ , Fill Factor FF and conversion Efficiency as function of the a-Si:H(p+) and a-Si:H(n+) layer thickness.

**III. 4. Effect of p-type and n-type doping concentrations layers**

Fig. 6 shows the dependency of solar cell parameters on the doping concentration of the p-layer and n-layer for our cell structure. We can see that when the doping concentration of a-Si:H(p+) increases, the efficiency also increases but the optimal value which can be choose is  $5 \times 10^{19} \text{cm}^{-3}$  because a larger acceptor concentration than this is difficult to obtain in the laboratory [11]. The optical and structural properties start to change significantly about a concentration of  $3 \times 10^{20} \text{cm}^{-3}$ . The optimal Voc value of 0.896V and FF of 84.2% are obtained for this acceptor concentration value. In contrast, the current density Jsc decreases only about 1% from  $33.02 \text{mA/cm}^2$  to  $32.946 \text{mA/cm}^2$ .

Due to the passivation effect of i-layer, the fill factor can be further increased. This effect can be shown in Fig. 7 where the FF and Efficiency are plotted as function of i-layer thickness. Thus the efficiencies of our best heterostructure solar cells using n-type substrates can reach 25.021%, the Fill Factor value 0.844, the Jsc  $32.948 \text{mA/cm}^2$  and the Voc 0.899V.

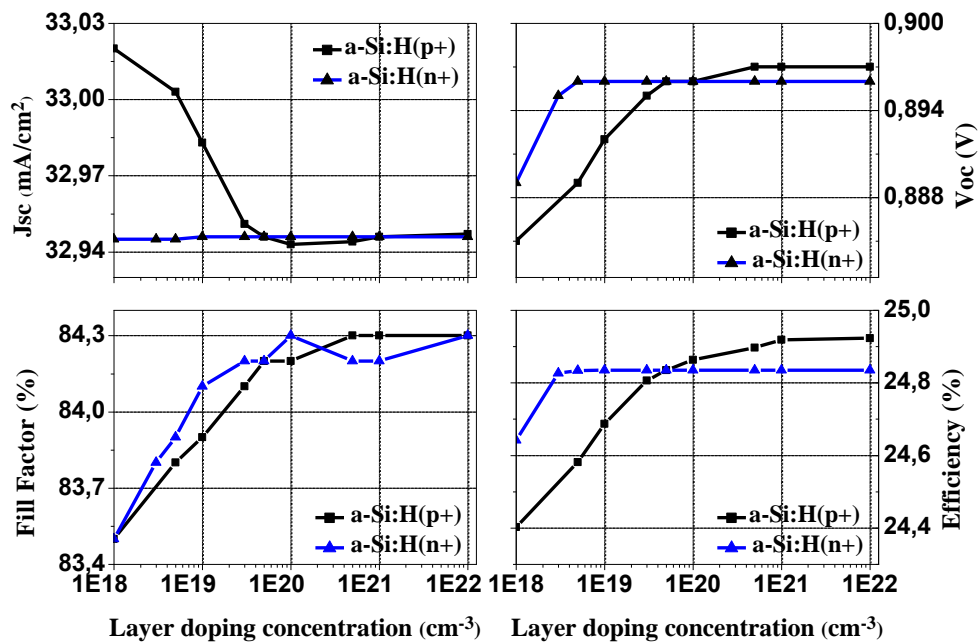


Fig. 6. Current density Jsc, Open-circuit voltage Voc, Fill Factor FF and conversion Efficiency as function of the a-Si:H(p+) and a-Si:H(n+) layer thickness.

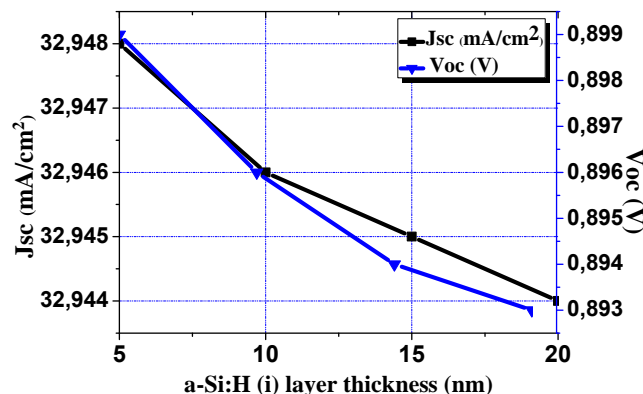


Fig. 7. Current density and conversion efficiency as function of the a-Si:H(i) layer thickness.

Once we have optimal values for Thickness and doping concentrations of the simulated device, the best solar cell structures is drawn in Fig. 8 for obtaining their short-circuit current density Jsc, open-circuit voltage

Voc, Fill Factor (FF) and efficiency. As it can be seen, high open-circuit voltage Voc of 0.899V is achieved and efficiency up to 25.021% is obtained.

Fig. 9 shows the Quantum Efficiency (QE) spectra of the best simulated heterojunction silicon solar cells as function of the wavelength. For the short wavelength range from 300nm to 500nm, losses increases due to the significant optical absorption in the a-Si emitter layer. However, the spectral response is very high at the wavelength between 500 and 800 nm. Thus, the QE loss in the blue region of the Si hetero junction solar cell using a n-type substrate is very low. The QE decreases again for the long wavelength region (> 800 nm) due to the back surface recombination.

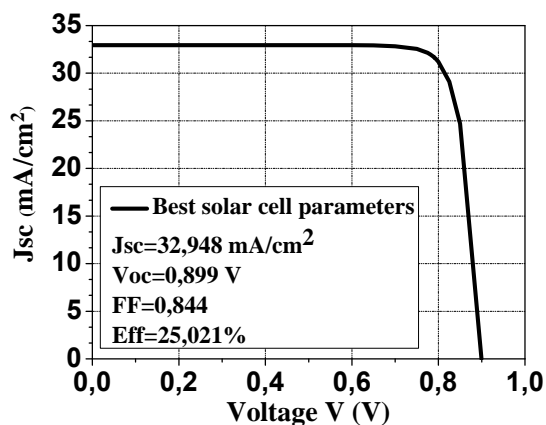


Fig. 8. Current density vs voltage (J-V) curves of the best Heterojunction solar cells.

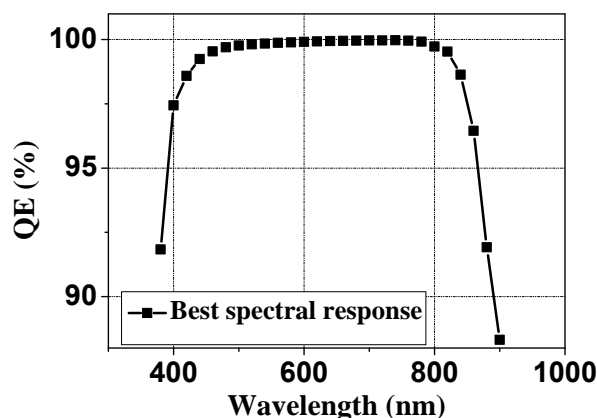


Fig. 9. QE spectrum of the best Heterojunction solar cells as function of the wavelength.

#### IV. CONCLUSION

In this work we focus on amorphous/crystalline heterostructure solar cell based on n-type crystalline wafer. The influence of various parameters on the solar cell performance was investigated using AMPS simulation program under AM1.5 solar spectrum and at room temperature. A particular choice of optimal values parameters for this layers device leads to our best TCO/ a-Si:H(p)/ a-Si:H(i)/ c-Si(n)/ a-Si:H(i)/ a-Si:H(n)/Al hetero-structure solar cells. A high photovoltaic conversion efficiency of 25.021% can be reached and an open-circuit voltage Voc value of 0.899V will be obtained.

#### Acknowledgements

The authors would like to thank Professor S. Fonash of the Pennsylvania State University for providing the AMPS-1D program used in the simulations.

#### REFERENCES

- [1]. Wang TH, Page MR, Iwaniczko E, Levi DH, Yan Y, Branz HM, et al. Toward better understanding and improved performance of silicon heterojunction solar cells. 14th Workshop on Crystalline Silicon Solar Cells and Modules, Winter Park, Colorado, USA, 8-11 August (2004).
- [2]. Tucci M, Noce MD, Bobeico E, Roca F, Cesare GD, Palma F. Comparison of amorphous/crystalline heterojunction solar cells based on n- and p-type crystalline silicon. *Thin Solid Films*, (2004); 355:451-2.
- [3]. Mehdi Hamid Vishkasougheh, Bahadir Tunaboylu. Simulation of high efficiency silicon solar cells with a heterojunction microcrystalline intrinsic thin layer. *Energy Conversion and Management*, (2013); 141-146.
- [4]. Sawada T. High-efficiency a-Si/c-Si heterojunction solar cell. *Proceeding of the IEEE 1st World Conference on Photovoltaic Energy Conversion*, Hawaii, USA, (1994); 1219-1226.
- [5]. Taguchi M, Kawamoto K, Tsuge S, Baba T, Sakata H, Morizane M, Uchihashi K, akamura N, Kiyama S, Oota O. HITTM cells high-efficiency crystalline Si cells with novel structure. *Progress in Photovoltaics: Research and Applications*, (2000); 8: 503-513.
- [6]. Pla J, Centurioni E, Summonte C, Rizzoli R, Migliori A, Desalvo A, Zignani F. Homojunction and heterojunction silicon solar cells deposited by low temperature-high frequency plasma enhanced chemical vapour deposition. *Thin Solid Films*, (2002); 405: 248-255.
- [7]. Shui-Yang Lien1, y and Dong-Sing Wu. Simulation and Fabrication of Heterojunction Silicon Solar Cells from Numerical Computer and Hot-Wire CVD. *Prog. Photovolt: Res. Appl.* (2009).

- [8]. Cleef MWM, Rath JK, Rubinelli FA, Werf CHM, Schropp REI, Weg WF. Performance of heterojunction p<sub>n</sub> microcrystalline silicon n crystalline silicon solar cells. *Journal of Applied Physics*, (1997); 82: 6089– 6095.
- [9]. Jagannathan B, Anderson WA. Defect study in amorphous silicon/crystalline silicon solar cells by thermally stimulated capacitance. *Journal of Applied Physics*, (1997); 82: 1930–1935.
- [10]. Voz C, Martin I, Orpella A, Puigdollers J, Vetter M, Alcubilla R, Soler D, Fonrodona M, Bertomeu J, Andreu J. Surface passivation of crystalline silicon by Cat-CVD amorphous and nanocrystalline thin silicon films. *Thin Solid Films*, (2003); 430: 270–273.
- [11]. Mishima T, Taguchi M, Sakata H, Maruyama E. Development status of high-efficiency HIT solar cells, *Solar Energy Materials & Solar Cells*, (2011); 95: 18–21.
- [12]. Jan Schmidt, Mark Kerr and Andres Cuevas. Surface passivation of silicon solar cells using plasma-enhanced chemical-vapour-deposited SiN films and thin thermal SiO<sub>2</sub>/plasma SiN stacks. *Semiconductor Science and Technology*, 16 (2001) 164–170.
- [13]. Kerr MJ, Cuevas. A Very low bulk and surface recombination in oxidized silicon wafers. *Semiconductor Science and Technology*, (2002) 17:35–38.
- [14]. Wim Soppe, Henk Rieffe and Arthur Weeber. Bulk and Surface Passivation of Silicon Solar Cells Accomplished by Silicon Nitride Deposited on Industrial Scale by Microwave PECVD. *Progress in Photovoltaics Research and Applications*, (2005); 13:551–569.
- [15]. Kerr MJ, Cuevas A. Recombination at the interface between silicon and stoichiometric plasma silicon nitride. *Semiconductor Science and Technology*, (2002); 17:166–172.
- [16]. Norberto HC, Arturo MA. *Sol Energy Mater Sol Cells*, (2010); 94:62–7.
- [17]. M.M. de Lima Jr., F.C. Marques. On the doping mechanism of boron-doped hydrogenated amorphous silicon deposited by rf-co-sputtering. *Journal of Non-Crystalline Solids*, (2002) 605-609.
- [18]. D. Bjelopavlić, Danijela Pantić, B. Đorđević, D. Pantić. Simulation of hetero-junction silicon solar cells. *Contemporary Materials I–2*, (2010) Page 186 of 194.
- [19]. S. V. Fonash, J. Arch, J.Cuiffi, J. Hou, W. Howland, P. McElheny, A. Moquin, M. Rogosky, F. Rubinelli, T. Tran, and H. Zhu, A manual for AMPS-1D for windows 95/NT; a one-dimensional device simulation program for the analysis of microelectronic and photonic structures. Pennsylvania State University, USA (1997).
- [20]. A. N. H. Al-Ajili and S. C. Bayliss, *Thin Solid Films*, (1997) 305: 116-123.
- [21]. Martin I, Vetter M, Orpella J, Puigdollers J, Cuevas A, Alcubilla R Surface passivation of p-type crystalline Si by plasma enhanced chemical vapor deposited amorphous SiC<sub>x</sub>:H films. *Appl Phys Lett*. (2001) 79:2199–2201.
- [22]. Wolfgang Rainer Fahrner. *Amorphous Silicon / Crystalline Silicon Heterojunction Solar Cells*. Springer Briefs in Applied Sciences and Technology, (2011).